Size Dependence of the $2p_{3/2}$ and $3d_{5/2}$ Binding Energy Shift of Ni Nanostructures: Skin-Depth Charge and Energy Trapping

Yi Sun,[†] J. S. Pan,*[,†] J. G. Tao,[‡] Y. G. Nie,[§] C. H. A. Huan,[†,‡] Z. Zhang,[†] J. W. Chai,[†] D. Li,[†] S. J. Wang,[†] and Chang Q. Sun[§,∥,⊥]

*Institute of Materials Research and Engineering, A*STAR (Agency for Science, Technology and Research), 3 Research Link, Singapore 117602, Division of Physics and Applied Physics, School of Physical and Mathematical Sciences, Nanyang Technological University, SPMS-04-01, 21 Nanyang Link, Singapore 637371, School of Electrical and Electronic Engineering, Nanyang Technological University, Singapore 639798, and Key Laboratory of Low-Dimensional Materials and Application Technologies (Ministry of Education), Faculty of Science, Xiangtan University, Hunan 411105, China*

Received: March 12, 2009; Revised Manuscript Received: April 15, 2009

Interaction between the undercoordinated atoms at sites surrounding defects, at edges, or at surfaces has been recognized as the key to the unusual behavior of low-dimensional systems. However, determination of the binding energy of an isolated atom and its bulk shifts with a clear insight into the origin of the size effect has been a longstanding challenge. Here we show that a combination of the X-ray photoelectron spectroscopy and Auger electron spectroscopy, or Auger photoelectron coincidence spectroscopy (APECS), the band theory, and the recently developed bond order-length-strength (BOLS) correlation mechanism [Sun. *Prog. Solid State Chem.* **2007**, *35*, 1] has enabled us to gain quantitative information regarding the $L(2p_{3/2})$ and $M(3d_{5/2})$ energy levels of an isolated Ni atom and their bulk shifts by numerically analyzing the size dependence of these energy bands of Ni nanostructures. Meanwhile, the correlation between the Auger kinetic energy, E_K, and the APECS-involved L and M lines has been first established, clarifying that the energy shift of the Auger parameter, or the sum of the absolute energy shift of the E_K and E_L, is twice that of the M level, E_M. Findings affirmed that the size-induced core-level shifts of nanostructures originate from the broken-bond-induced local strain and the associated skin-depth quantum trapping, which results in deeply- and densely trapped charge and energy in the surface skin of two interatomic spacings in depth.

I. Introduction

Interatomic interaction plays a pivotal role in differentiating the behavior of a bulk solid from that of individually isolated constituent atoms, such as mechanical strength, chemical and thermal stability, lattice vibration, photon emission and absorption, and electronic, magnetic, and dielectric properties.[1] The energy levels of an isolated atom evolve into energy bands upon bulk formation associated with an energy shift toward lower binding energy (or a positive shift to higher absolute value); phase transition can only happen to the bulk rather than to a single atom; and unlike its bulk counterparts, an isolated atom does not have a detectable melting point or mechanical strength. Without interatomic bonding, neither solids nor liquids could form. The energy distribution of the valence electrons also determines the catalytic behavior of metallic nanocrystals.[2] Recently, the interaction between the undercoordinated atoms at sites surrounding defects, at edges, or at surfaces of skin depth has been recognized as the key to understanding the intriguing behavior of low-dimensional systems such as atomic chains, nanoribbons, nanotubes, nanowires, nanograins, nanocavities, and the surface skin of a bulk specimen in various properties. However, quantifying the individual energy levels due to intra-atomic trapping of an isolated atom and their shifts upon bulk formation due to interatomic binding as well as the effects of crystal-field screening and valence recharging during reaction in a nanostructured solid has been a longstanding pursuit.

The broad peak of the density-of-states (DOS) of a certain energy band results from intra-atomic trapping, crystal binding, and the effects of crystal orientation, surface relaxation, nanosolid formation, or surface passivation, which can be measured using X-ray photoelectron spectroscopy (XPS) for the intermediate energy levels or using Auger electron spectroscopy (AES) for much deeper energy levels. The evolution of the valence DOS can be monitored by ultraviolet spectroscopy or scanning tunneling spectroscopy. When a solid grows from an atomic scale to macroscopic with dimension K, the atomic energy levels expand to bands with prominent peaks, known as the core band characteristic energies. Meanwhile, the center of the band will shift in a way that depends on the crystal binding energy in terms of overlap and exchange integral. K, the dimensionless form of size, is the number of atoms lined along the radius of a spherical dot or across the thickness of a plate. When the solid grows to form a primitive unit cell or a monatomic chain, the energy of a certain level denoted with quantum number ν drops from the initial $E_\nu(1)$ value for an isolated atom sharply to a (absolute) maximum and then restores in a K^{-1} fashion to the bulk value of the energy shift,[3] $\Delta E_\nu(\infty)$. From X-ray absorption spectroscopy measurements, Reif et al.[4] have confirmed that

* To whom correspondence should be addressed. E-mail: js-pan@imre.a-star.edu.sg.
† A*STAR.
‡ School of Physical and Mathematical Sciences, Nanyang Technological University.
§ School of Electrical and Electronic Engineering, Nanyang Technological University.
∥ Xiangtan University.
⊥ E-mail: ECQSun@ntu.edu.sg.

10.1021/jp902405q CCC: $40.75
Published on Web 06/02/2009

the occupied DOS of the E_{2p} level shifts monotonically from the $E_{2p}(1)$ level of an isolated Cr atom at 573.5 eV, by ~0.9 eV, to the E_{2p} (13 atoms) at 574.4 eV. Size-induced positive core-level shift of nanostructures has been frequently observed by many researchers.[5–10] The additional positive core-level shift with respect to that of the bulk counterpart indicates particularly the enhancement of interatomic bonding between the undercoordinated atoms of nanostructures.

Sophisticated models have been developed to explain the physical origins of the surface- and size-induced core-level shift. The observed energy shifts are often attributed to the "final (ionized)- initial (neutralized) state" effect[11] or the "poor screening" effect of the core−hole.[12] However, experimental investigations[13] have shown that the "final−initial state" effect cannot account for all observations, and a metal-to-nonmetal transition mechanism was suggested to occur with a progressive decrease in cluster size.[12] Despite intensive theoretical and experimental investigations, a number of issues still remain challenging. First, the correlation between the Auger kinetic energy and the energy shifts of the Auger photoelectron coincidence spectroscopy (APECS) involved energy levels, i.e., L, M, and E_K, needs to be established. Second, the new degree-of-freedom of size should allow us to quantitatively discriminate the binding energy from the intra-atomic trapping effect. Third, determination of the $E_v(1)$ for an isolated atom and its bulk shift is highly desired yet remains beyond the scope of available approaches. Finally, only a few examples have been available regarding the electronic behavior of Ni nanostructures on oxide surfaces and theoretical reproduction of the measured size dependence is still lacking.[14,15]

Although the chemistry and physics of materials at surfaces and on a nanometer scale has been extensively investigated, the behavior of electrons surrounding the undercoordinated atoms has not been fully understood. The objective of this work is to show that we are able to establish the correspondence between the APECS-involved energy levels and their physical origins through analysis of the size dependence of the energy shifts of Ni nanostructures deposited on TiO_2 substrates. The combination of solid size variation, the APECS technique, and the bond order−length−strength (BOLS) correlation has led to an improved understanding of the energetics of the APECS-involved energy levels of an isolated Ni atom, as well as the corresponding bulk shifts of these energy levels, with a consistent insight into the physical origin of the size effect on the electronic energies of nanostructures. It is emphasized that the broken-bond-induced local strain and skin-depth quantum trapping dictate the observed energy shifts in XPS, AES, and APECS.

II. Principles

A. BOLS Correlation: Broken-Bond-Induced Strain and Quantum Trapping. The BOLS correlation mechanism[1] indicates that if one bond breaks, the remainder between the undercoordinated atoms becomes *shorter and stronger*. Consequently, local strain and quantum trapping will occur, together with densification of charge and energy at sites surrounding an atomic defect, the surface, or the skin of a nanostructure. This broken-bond-induced local strain and skin-depth quantum trapping cause perturbation to the Hamiltonian and related properties, such as the band gap opening and core level shift.

Figure 1a shows the atomic arrangement at a flat surface with adatoms or edge atoms labeled with S_{e1} and S_{e2}, the outermost and the second atomic layers labeled with S_1 and S_2, and the bulk labeled with B. Panel b shows the corresponding interatomic potentials between the undercoordinated atoms. The coordinate at the potential valley (C_i, C_i^{-m}) corresponds to the dimensionless form of bond length and energy ($d_i = C_i d$; $E_i = C_i^{-m} E_b$) at equilibrium, with C_i being the bond contraction coefficient, $C_i = 2\{1 + \exp[(12 - z_i)/(8z_i)]\}^{-1}$. E_b and d are the corresponding bond energy and bond length in the bulk. z_i is the effective coordination number of an atom in the ith atomic layer counted from the outermost layer to the center of the solid. The bond nature indicator, m, is not a freely adjustable parameter.[1] The difference between a nanostructure and a flat surface is that the nanosized specimen possesses a nonzero curvature and the tunable fraction of the undercoordinated atoms while the curvature of a flat surface is zero with a fixed fraction of undercoordinated atoms in the outermost two atomic layers. Therefore, a surface and a nanostructure are substantially the same in nature.

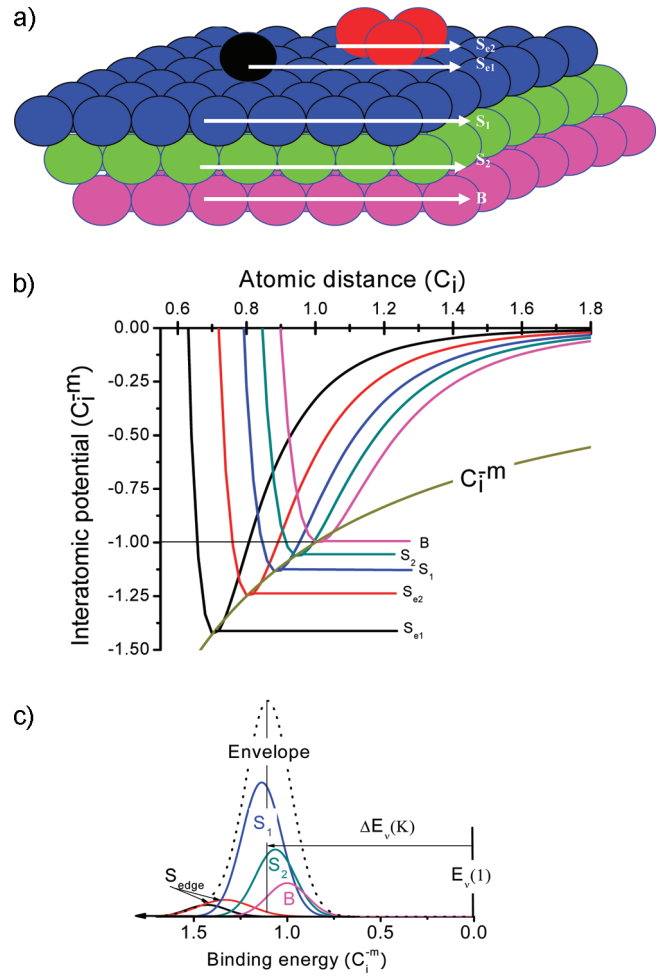

Figure 1. Illustration of the origin for the size- and surface-induced core level shift. (a) Atomic arrangement at a surface with irregularly grown adatoms (S_{e1}) and the edge atoms (S_{e2}). S_1, S_2, and B represent the outmost, the second, and the bulk components. (b) Bond order deficiency induced bond contraction and the associated interatomic potential depression. (c) Core level shift of each component and their convolution to form the envelope. The energy shift and the lowering of the atomic potential of each component satisfy $\Delta E_v(i)/\Delta E_v(B) = E_i/E_b = C_i^{-m}$ ($i = S_{e1}, S_{e2}, S_1, S_2$).

B. Energy Levels, Energy Bands, and Core Level Shifts. According to the band theory, the Hamiltonian and the associated electronic energy dispersion relation are given as[21]

$$\begin{cases} H = -\dfrac{\hbar^2\nabla^2}{2\mu} + V_{\text{atom}}(r) + V_{\text{cry}}(r) & \text{(single body Hamiltonian)} \\ E_\nu(k) = E_\nu(1) - \Delta E_\nu(K) + \Phi(k, R_{\text{L}}) & \text{(electronic energy dispersion)} \end{cases} \quad (1)$$

The intra-atomic trapping potential, $V_{\text{atom}}(r)$, determines the νth energy level of an isolated atom, $E_\nu(1)$, which remains a constant disregarding external conditions. K is the dimensionless form of solid size. The crystal potential $V_{\text{cry}}(r)$ determines the core level shift, $\Delta E_\nu(K)$. The bandwidth or electronic kinetic energy, $\Phi(k,R_{\text{L}})$, depends on the crystal geometry (R_{L} is the lattice constant), the wave vector k, and the overlap integral. These quantities are expressed as follows:

$$\begin{cases} E_\nu(1) = \langle\phi_\nu(r)|V_{\text{atom}}(r)|\phi_\nu(r)\rangle & \text{(core level energy)} \\ \beta = \langle\phi_\nu(r)|V_{\text{cry}}(r)|\phi_\nu(r)\rangle \propto \langle E_{\text{b}}\rangle & \text{(exchange integral)} \\ \gamma = \langle\phi_\nu(r)|V_{\text{cry}}(r)|\phi_\nu(r')\rangle \propto \langle E_{\text{b}}\rangle & \text{(overlap integral)} \\ \Delta E_\nu(K) = -(\beta + c\gamma) \propto \langle E_{\text{b}}\rangle & \text{(core level shift)} \end{cases} \quad (2)$$

$\phi_\nu(r)$ ($r \neq r'$) is the specific Bloch wave function at a specific site r. One needs to note that the exchange and overlap integrals β and γ are proportional to the cohesive energy per bond, $\langle E_{\text{b}}\rangle$. Therefore, the core level shift is dominated intrinsically by the bond energy. Any perturbation to β and γ will cause the energy to shift. The $\Delta E_\nu(K)$ can be uniquely tuned by modifying the bond energy $\langle E_{\text{b}}\rangle$ or the crystal field if the Bloch wave function were assumed to remain unchanged. The parameter c is a constant whose value depends on the crystal geometry. Bond relaxation through solid size reduction and bond nature alteration through chemical reaction are possible ways of modifying the crystal potential and hence the shift of the core levels.

As the core level shift is proportional to the cohesive energy per bond that can be enhanced by bond order loss, the energy level of a small substance will shift to lower binding energy. The observed DOS of a specific energy band can be decomposed into the S_{edge} (S_{e1}, S_{e2}), S_1, S_2, and B components, as illustrated in Figure 1c, corresponding to contributions from the adatoms or edge atoms, the outermost atoms, the second surface layer, and the remaining of the bulk in an order from the lower (larger in absolute value) to higher binding energies. The energy shift of the components relating to the undercoordination component will be more positive than those of others with higher coordination numbers. Although the number of peaks that the spectra can be decomposed into can be of an arbitrary value, the above-mentioned components make up the only physically justifiable number because evidence[1,20] exists for bond contraction in only the outermost two atomic layer spacings, hence supporting the existence of S_1 and S_2 components with S_{e} as an addition subject to the smoothness of the surface.

C. Auger Process and APECS Lines. Figure 2 shows the energy diagram of a solid growing from one atom to a solid containing N atoms, $N(K)$, or alternatively, of size K. There are two stages for the energy shift: when the solid grows from one atom to a unit cell, all the energy levels shift sharply to their maximum values;[4] with further growth of the solid to an infinitely large specimen, all the energy levels recover gradually from their maxima to the bulk values in a manner that is proportional to the inverse of its size, K^{-1}. With a given size, the magnitude of the energy shift varies from level to level because electrons in the higher energy levels

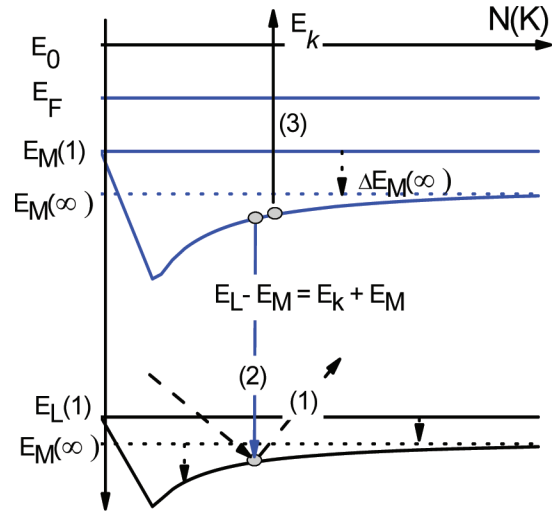

Figure 2. Schematic illustration of (i) the energy levels of an isolated atom $E_\nu(1)$ (ν = L and M), (ii) size-induced energy shifts of a solid containing N atoms or with dimensionless form of size $N(K)$, $E_\nu(K) - E_\nu(1)$, and (iii) the energy conservation of the APECS involved energy levels: $E_{\text{K}} + E_{\text{M}} = E_{\text{L}} - E_{\text{M}}$. $E_\nu(\infty) - E_\nu(1)$ is the bulk shift. The $E_{\text{M}}(K)$ and $E_{\text{L}}(K)$ are measurable while the $E_{\text{M}}(1)$ and $E_{\text{L}}(1)$ and their bulk shift (dotted lines) can be determined using the current approach.

experience a stronger interatomic potential than electrons in the deeper ones due to the screening effect. The energy shifts of the upper levels are therefore expected to be greater than those located deeper.

Figure 2 also illustrates the Auger process and the correlation between the Auger kinetic energy, E_{K}, and the APECS-involved L($2p_{3/2}$) and M($3d_{5/2}$) lines. In an Auger process, a photoelectron is emitted (process labeled 1) from the deeper L initial level upon the excitation of the sample by an energetic electron or X-ray beam, leaving an electronic hole in the L level. This process of core-ionization causes a relaxation of all the energy levels due to the weakening of the screening effect of both the intra-atomic potential on electrons in the outer shells and the interatomic binding on the ion core. An electron then transitions spontaneously from the relaxed upper M level to the hole in the deeper L level (process labeled 2). The energy released by this transition excites another electron in the further relaxed M level, forming the Auger electron (process labeled 3). The Auger electron overcomes the binding energy E_{M} and escapes from the solid with the Auger kinetic energy E_{K}.

1. Energy Conservation in the Auger Process. Conventionally, the observed energy shifts of the E_{L} and E_{K} lines in the APECS experiments are often correlated by the Auger parameter,[16] $\alpha' = E_{\text{K}} + E_{\text{L}}$, and the Wagner plot[17] of ΔE_{K} versus ΔE_{L}, without the M level being involved.[18] The Wagner plot shows the linear interdependence of ΔE_{K} and ΔE_{L} in absolute values with reference to the bulk shifts that are deemed as zero. The energy shift of the Auger parameter $\Delta\alpha'(\infty)$ is also assumed to be zero. In reality, however, the energy shifts $\Delta E_{\text{K}}(1)$, $\Delta E_{\text{L}}(1)$, and $\Delta\alpha'(1)$ are zero. The correct reference point for the energy shift of all energy levels should be the absolute values of an isolated atom instead of those of the bulk sample. Unfortunately, this problem cannot be solved unless the binding energy of an isolated atom is determined.

If the absolute values of energies are considered, one can find that the sum of E_{K} and E_{M} equals the energy difference between the L and the M levels. That is, in the APECS process, the energy is conserved. This rule of energy

conservation has been undermined until the present. This rule of energy conservation together with the Auger parameter, the extended Wagner plot, and the screening coefficient can be formulated as

$$\begin{cases} E_K(K) + E_M(K) = E_L(K) - E_M(K) & \text{(APECS energy conservation rule)} \\ \alpha'(K) = |E_K(K)| + E_L(K) & \text{(Auger parameter)} \\ \dfrac{\Delta E_M(K)}{\Delta E_M(\infty)} = \alpha_{ML}\dfrac{\Delta E_L(K)}{\Delta E_L(\infty)} & \text{(extended Wagner plot)} \\ \beta_{ML} = \Delta E_M(\infty)/\Delta E_L(\infty) & \text{(screening coefficient)} \end{cases} \quad (3)$$

The energy conservation is subject to the assumption that the relaxation energy is negligible. In fact, the relaxation energy exits throughout a photoelectron emission measurement disregarding the solid size, which can be treated as one of the artifacts of the facility and could be treated as background in the experiment. Furthermore, the relaxation process proceeds in the velocity of the electromagnetic field, which is hardly detectable. The coefficient α_{ML} in the extended Wagner plot represents the effect of valence recharging due to chemical reaction on the shifts of the two energy levels. Ideally, $\alpha_{ML} = 1$, if no chemical reaction is involved. The screening coefficient, $\beta_{ML} > 1$, represents the ratio of binding energies of two separate levels in a bulk of an elemental solid. All the νth energy levels shift from the $E_\nu(1)$ of an isolated atom, instead of the bulk. The relative shift of $\Delta E_\nu(K)/\Delta E_\nu(\infty)$ is more meaningful than the absolute shift $\Delta E_\nu(K)$, as the relative shift corresponds to the modification of the binding energy through changing the size of a solid. Therefore, the extended Wagner plot and the screening coefficient would be more convenient and useful than the traditional Wagner plot that only correlates the absolute shifts of the Auger kinetic energy and the lower binding energy. According to the measurements and energy conservation rule, $\Delta E_K(K) = \Delta E_L(K) - 2\Delta E_M(K) < 0$, when the E_L and E_M are shifted downward simultaneously.

2. Correlation between the E_K, E_L, and E_M. Considering the simultaneous energy shifts of the APECS-involved energy levels with respect to the corresponding energy levels of an isolated atom, one can derive that the energy shift of the Auger parameter is actually twice that of the M level.

$$\begin{cases} \Delta E_K(K) + \Delta E_M(K) = \Delta E_L(K) - \Delta E_M(K) & \text{(energy conservation)} \\ \Delta\alpha'(K) = |\Delta E_K(K)| + \Delta E_L(K) = -\Delta E_K(K) + \Delta E_L(K) & \text{(Auger parameter)} \end{cases}$$

or

$$\Delta\alpha'(K) = -[\Delta E_L(K) - 2\Delta E_M(K)] + \Delta E_L(K) = 2\Delta E_M(K) \quad (4)$$

D. Correlation between the Core Level Shift and the Local Lattice Strain. According to the energy band theory and the BOLS correlation, solid size reduction or surface relaxation could perturb the overall crystal potential, $V_{cry}(r)$, in the Hamiltonian of an extended solid,[19]

$$V(\Delta_i) = V_{atom}(r) + V_{crys}(r)[1 + \Delta_H] \quad (5)$$

The Δ_H corresponds to the Hamiltonian perturbation that sums over only the outermost three atomic layers, as the atoms in the core interior do not experience coordination deficiency, as recently confirmed by Huang et al.[20] for gold nanoclusters. Using a core−shell structural configuration, the perturbation is given by[1]

$$\begin{cases} \Delta_H = \sum_{i\le 3}\gamma_i\Delta_i = \dfrac{\tau}{K}\sum_{i\le 3}C_i\Delta_i = \dfrac{\tau}{K}\Delta'_H & \text{(nanostructure)} \\ \Delta_i = C_i^{-m} - 1 & \text{(surface component)} \end{cases} \quad (6)$$

where $\sum_{i\le 3}C_i\Delta_i = \Delta'_H$ and $\gamma_i = \tau C_i K^{-1}$, being the surface-to-volume ratio, depends on the dimensionality, τ, and size, K. $\tau = 1$, 2, and 3 corresponds, respectively, to the dimensionality of a thin plate, a cylindrical rod, and a spherical dot. Δ_H originates from the broken-bond-induced bond contraction ($d_i = C_i d$) and the associated bond energy gain ($E_i = C_i^{-m}E_b$) in the outermost three ($i \le 3$) atomic layers. $\Delta_H > 0$ indicates that the interatomic trapping potential between undercoordinated atoms is deepened. As a consequence, all the energy levels at the specific sites undergo positive shifts accordingly.

Incorporating the BOLS correlation into the band theory with the surface-induced Hamiltonian perturbation, we have the form for the energy shift of a specific energy level of a nanostructure or a surface component,

$$\Delta E_\nu(K) = E_\nu(K) - E_\nu(1) = \Delta E_\nu(\infty)(1 + \Delta_H) = [E_\nu(\infty) - E_\nu(1)](1 + \Delta_H)$$

or

$$\frac{E_\nu(K) - E_\nu(1)}{E_\nu(\infty) - E_\nu(1)} = 1 + \begin{cases} \Delta_H = \tau\Delta'_H/K & \text{(nanostructure)} \\ \Delta_i = C_i^{-m} - 1 & \text{(surface component)} \end{cases}$$

or, alternatively,

$$\frac{E_\nu(K) - E_\nu(\infty)}{E_\nu(\infty) - E_\nu(1)} = \begin{cases} \Delta_H = \tau\Delta'_H/K & \text{(nanostructure)} \\ \Delta_i = C_i^{-m} - 1 & \text{(surface component)} \end{cases} \quad (7)$$

Similarly, we can establish the size dependence of the mean lattice strain of a crystal with dimensionality τ based on the BOLS correlation and core−shell configuration:[1]

$$\frac{\Delta d}{d} = \Delta_d = \sum_{i\le 3}\gamma_i(c_i - 1) = \frac{\tau}{K}\sum_{i\le 3}c_i(c_i - 1) = \frac{\tau\Delta'_d}{K} \quad (8)$$

The size-induced core level shift and lattice strain of a nanostructure are thus correlated through eqs 7 and 8. The Δ'_H and the Δ'_d originate the strain and the energy perturbation; the surface-to-volume ratio (shape and size τ/K) determines the extent of change. If $C_i = 1$, the Δ'_d and Δ'_H will be zero; neither lattice strain nor core-level shift will happen. If all bonds in the crystal contribute to the strain and energy shift, the summation

will proceed over all the atomic layers; the surface-to-volume ratio becomes a constant. In such a situation, no size dependence will be observed. Therefore, the measured K^{-1} dependence of the energy shift and the lattice strain indicates clearly the dominance of the strained bonds in the surface shell of limited thickness in determining the size-induced change. Hence, the broken-bond-induced local strain and quantum trapping in the outermost three atomic layers[20] are the key to the observations while bonds between the fully coordinated atoms in the core interior remain as they are in the bulk, making no contribution to the size effect.[1,24]

E. Estimation of $E_\nu(1)$ and $\Delta E_\nu(\infty)$. For a surface, the core-level shift and the interatomic bond energy are correlated to the corresponding bulk values in the following way:

$$\Delta E_\nu(i):\Delta E_\nu(B) = E_i:E_b = C_i^{-m} \quad (i = S_{e1}, S_{e2}, S_1, S_2)$$

This rule provides a constraint for the surface core-level shift decomposition:

$$\frac{E_\nu(i) - E_\nu(1)}{E_\nu(i') - E_\nu(1)} = \frac{C_i^{-m}}{C_{i'}^{-m}} \quad (i \neq i') \tag{9}$$

For nanostructures, measurements[5–10] revealed that the size-induced energy shifts follow a scaling relation,[22,23] $E_\nu(K) = A + BK^{-1}$, where A and B are the Y-axis intersection and the slope of the linear dependence, respectively. Combining this scaling relation with eq 7 yields

$$E_\nu(K) = \begin{cases} E_\nu(\infty) + [E_\nu(\infty) - E_\nu(1)]\tau\Delta'_H K^{-1} & \text{(BOLS theory)} \\ A + BK^{-1} & \text{(measurement)} \end{cases} \tag{10}$$

Equating the BOLS expectations with measurement results, we have

$$\begin{cases} B = [E_\nu(\infty) - E_\nu(1)]\tau\Delta'_H \\ A = E_\nu(\infty) \end{cases}$$

and

$$\begin{cases} E_\nu(1) = A - \dfrac{B}{\tau\Delta'_H} & \text{(atomic energy level)} \\ \Delta E_\nu(\infty) = \dfrac{B}{\tau\Delta'_H} & \text{(bulk shift)} \end{cases} \tag{11}$$

Therefore, given the linearization data of A and B of the measured shape-and-size dependence of the energy shift of a specific energy level, we can readily calculate the energy level of an isolated atom and its bulk shift.

III. Experimental Procedure

The experiments were performed using the VG ESCALAB 220i-XL instrument (base pressure $< 5 \times 10^{-10}$ mbar) with a monochromatic Al Kα (1486.7 eV) X-ray source. The XPS binding energy was calibrated using pure gold, silver, and copper standard samples by setting the Au $4f_{7/2}$, Ag $3d_{5/2}$, Cu $2p_{3/2}$ peaks and Ni Fermi edge at a binding energy (BE) of 83.98 ± 0.02 eV, 368.26 ± 0.02 eV, 932.67 ± 0.02 eV, and 0.00 ± 0.02 eV, respectively. All spectra were recorded in the constant pass energy mode with the pass energy set at 20 eV and a step width of 0.1 eV. In this experiment, Ni clusters were grown on TiO_2 substrates. Clean TiO_2 surfaces were obtained by repeated cycles of Ar^+ sputtering and ultrahigh vacuum (UHV) annealing. The cleanliness and chemical state of the substrate were ascertained by verifying the high-sensitivity and high-resolution XPS spectra measured. Subsequently, Ni was deposited by an Omicrometer EFM3 e-beam evaporator in the preparation chamber. The e-beam evaporator deposition rate was calibrated by Rutherford backscattering measurements. The film thickness was achieved through deposition time control.[25] The thickness of Ni is quoted in units of monolayer (ML), that is defined as the same packing density of the Ni(111) surface. Here we initially assume the film growth to be of a layer-by-layer manner, but further justification through calculations would be more encouraging because of a lack of visual evidence.

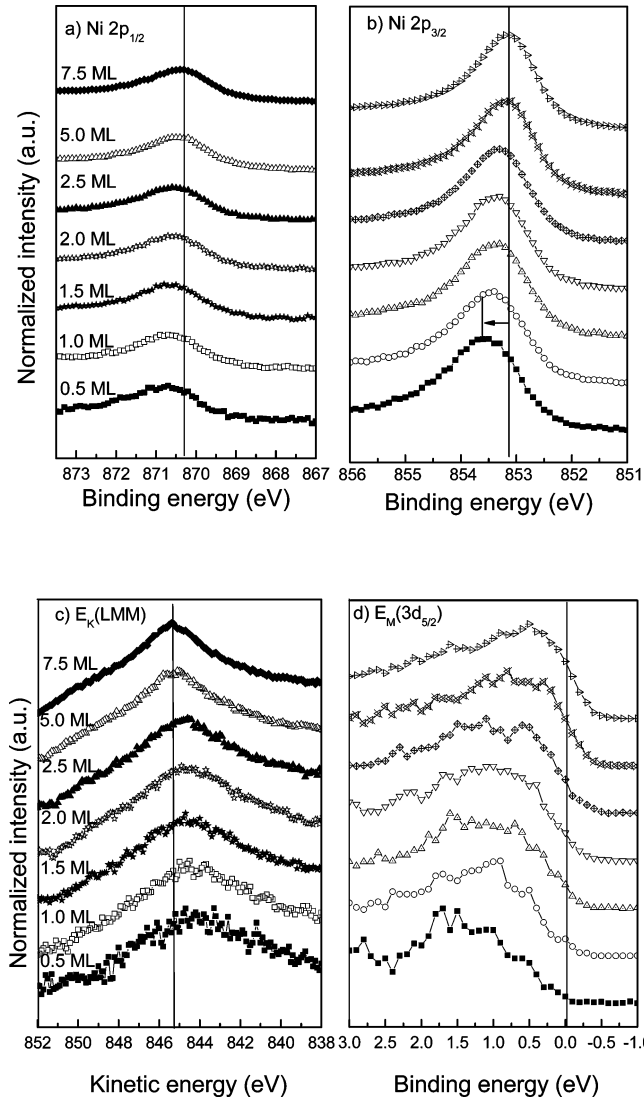

Figure 3. Normalized thickness-dependent energy spectra of (a) $2p_{1/2}$, (b) $2p_{3/2}$, (c) Auger kinetic energy, and (d) $3d_{5/2}$ band for Ni films deposited on a TiO_2 substrate show a definite positive shift of the L and M lines and a negative shift to the kinetic energy due to the broken-bond-induced local strain and quantum trapping. The ML is calibrated in terms of the packing density of rutile TiO_2.

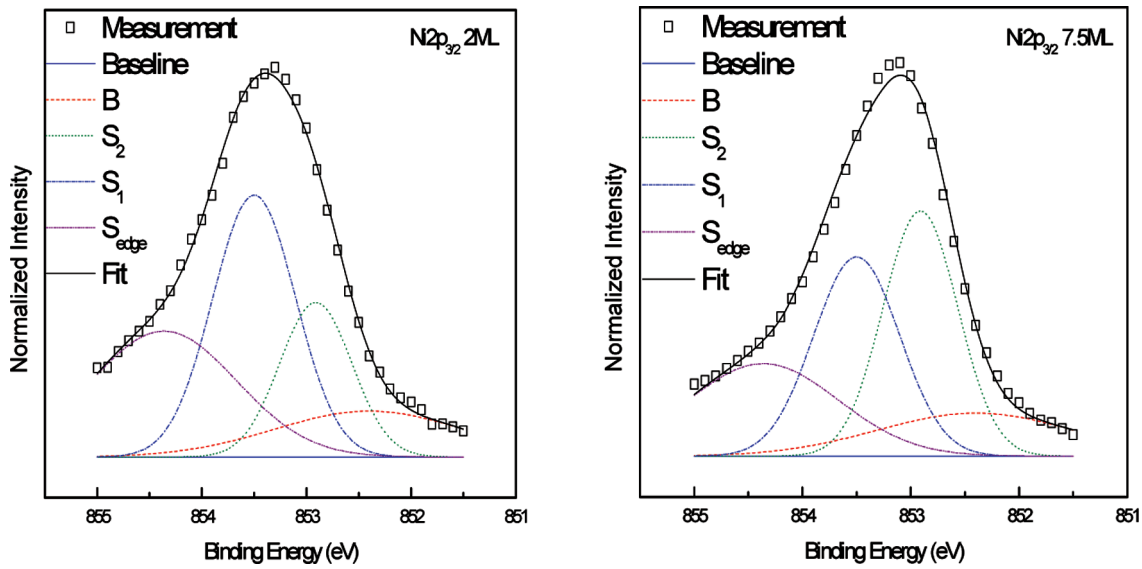

Figure 4. Comparison of the $2p_{3/2}$ band for (a) 7.5 ML and (b) 2 ML Ni films decomposed using four components, denoted S_{edge}, S_1, S_2, and B. The scattered squares are experimental data, and the lines are the fit components; the background is subtracted by the Shirley method. The resulting fit is superimposed on the data. The presence of the B feature in the 2 ML film indicates the possibility of an islandlike pattern of film growth, and the broad S_{edge} components indicate the presence of less than perfectly ordered structures. The reversal of the S_1 and S_2 peak intensities confirms the size-induced positive shift.

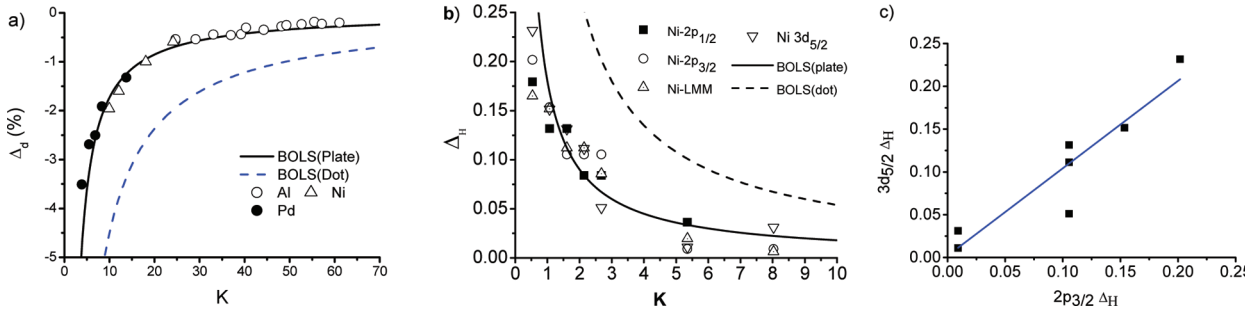

Figure 5. BOLS reproduction of the observed size dependence (scattered data) of (a) the mean lattice strain ($\Delta_d = \Delta d/d$) of Ni,[26] Al,[27] and Pd[28] nanostructures and (b) the relative energy shifts ($\Delta_H = [E_v(K) - E_v(1)]/[E_v(\infty) - E_v(1)]$ of the APECS involved energy levels with derived information listed in Table 1; $\tau = 3$ can be reproduced by adjusting the value of $E_v(1)$, as detailed in Table 1. (c) The extended Wagner plot of the M versus L energy shift with a slope of unity, indicating a negligible interface effect on the core level shift.

IV. Results and Discussion

A. APECS Spectra. As expected, the normalized energy spectra in Figure 3 show the positive shift of the (a) Ni-$2p_{1/2}$, (b) Ni-$2p_{3/2}$, and (d) Ni-$3d_{5/2}$ bands and a negative shift of the (c) Auger ($L_3M_{45}M_{45}$) kinetic energy when the film thickness is decreased. The broad Ni-$3d_{5/2}$ band should be an overlap of the $3d_{5/2}$ and 4s bands. This trend agrees with measurements of other surfaces and nanostructures[5–10,22,23] and the BOLS expectation of skin-depth quantum trapping. Each spectrum corresponds to a thickness (the thicknesses in Figures 3 are labeled in terms of the packing density of rutile TiO_2, 1.4×10^{15} atoms/cm^2, or its diameter of 0.267 nm, whereas the diameter of Ni, 0.249 nm, is used in subsequent calculations of K, which is in equivalent monolayers).

B. Decomposition of the APECS Spectra and Linearization of the $E_v(K)$. The normalized spectra were then decomposed using four Gaussian functions into the peaks for the components denoted as S_{edge}, S_1, S_2, and B, respectively, as shown in Figure 4 for the 2 ML and 7.5 ML samples. The reversal of the relative intensities of the S_1 and S_2 peaks for the 2 ML and the 7.5 ML indicates a positive shift because the APECS collects more information from the deeper layers for the thicker sample than for the thinner one. The presence of the B peak in the 2 ML sample indicates a possible island mode of thin film growth; otherwise, the B peak should be absent in a layer-by-layer mode of film growth. The broad S_{edge} peak indicates that the nanostructure is less than perfectly ordered with a certain number of edges and adatoms. Therefore, both cases of layer-by-layer and island growth modes have to be considered while analyzing the spectra. The different growth modes can be described by the shape or dimensionality factor, τ, which plays a role in calculating accurately the $E_v(1)$ value. It would be possible to determine the τ value using *in situ* scanning tunneling microscopy.

The binding energy at which the maximum peak sum intensity occurs is taken as the characteristic $E_v(K)$ for Ni films of different thicknesses. For each of the $2p_{1/2}$, $2p_{3/2}$, LMM, and $3d_{5/2}$ peaks, the series of $E_v(K)$ derived from the multipeak fitting is plot against K^{-1}. The linear fitting of the $E_v(K)$ vs K^{-1} curve gives the values of the intercept A and slope B, with the standard deviation from the fit as the error. With the given A and B values, we are able to calculate $E_v(1)$ and the corresponding bulk shift.

C. Estimation of $E_v(1)$ and $\Delta E_v(\infty)$. In the BOLS convention,[1] we took $z_1 = 4$ and $z_2 = 6$, $z_3 = 12$, and $m = 1$ (for metals) to obtain $C_1 = 0.88$, $C_2 = 0.94$, and $C_3 = 1$. Therefore, $\Delta'_1 = 0.12$, $\Delta'_2 = 0.06$, and $\Delta'_H = \Delta'_1 + \Delta'_2 = 0.18$. Similarly, Δ'_d is calculated as -0.162. Figure 5 shows the BOLS reproduction of the observed size dependence (scattered data)

TABLE 1: BOLS Theory Derived Information from the Matching of the Measured Thickness Dependence of the APECS Lines for Ni Films[a]

	$A = E_\nu(\infty)$	B	$E_\nu(1)$ ($\tau = 1$)	$E_\nu(\infty) - E_\nu(1)$ ($\tau = 1$)	$E_\nu(1)$ ($\tau = 3$)	$E_\nu(\infty) - E_\nu(1)$ ($\tau = 3$)
E-$2p_{1/2}$	879.32 ± 0.04	0.38 ± 0.08	868.23	2.10	869.62	0.70
E-$2p_{3/2}$	853.18 ± 0.04	0.37 ± 0.08	851.10	2.08	852.49	0.69
E-$3d_{5/2}$	5.49 ± 0.09	0.90 ± 0.17	0.51	4.99	3.83	1.66
E_K ($L_3M_{45}M_{45}$)	845.45 ± 0.13	-1.36 ± 0.23	853.02	−7.57	847.97	−2.52
	$\alpha = \lvert E\text{-}2p_{3/2}\rvert + \lvert E(L_3M_{45}M_{45})\rvert$			9.64		3.21
	$\alpha = 2 \times \lvert E\text{-}3d_{5/2}\rvert$			9.97		3.32

[a] The ML thickness is calibrated based on a Ni atom diameter of 0.249 nm. A and B correspond to the intercept and the slope of the fit to experimental data against $1/K$. $\Delta_H' = 0.18$, $\tau = 1$ and 3 correspond to layer-by-layer and island growth modes, respectively, which derives the different values of the $E_\nu(1)$ and its subsequence. The error bar is smaller than 0.3 unless it is given. The energy shifts of the Auger parameter derived from two different expressions are also compared.

TABLE 2: Decomposition Parameters for the $2p_{3/2}$ Lines of the 2 and 7.5 ML Samples[a]

K (ML)	S_{edge} ($E_{3/2}$/width)	S_{edge} area	S_1 ($E_{3/2}$/width)	S_1 area	S_2 ($E_{3/2}$/width)	S_2 area	B ($E_{3/2}$/width)	B area
2	854.36/31.63	0.54	853.49/0.93	0.64	852.91/0.81	0.33	852.40/2.13	0.04
7.5		0.39		0.48		0.52		0.02

[a] The component peak positions follow the relation $\Delta E_\nu(i):\Delta E_\nu(B) = C_i^{-m}$ ($i = S_{edge}, S_1, S_2$).

of (a) the mean lattice strain of Ni (calculated),[26] Al,[27] and Pd[28] (measured) nanostructures and (b) the energy shifts of the APECS involved three lines. Reproduction of the size-induced mean lattice strain of the three specimens indicates that the size effect on the surface bond length is universally true.[20] Figure 5b only compares the fitting to the situation of $\tau = 1$. $\tau = 3$ can also be fit by adjusting the $E_\nu(1)$ value in eq 7 in the process of fitting, $E_\nu(K) - E_\nu(\infty) = [E_\nu(\infty) - E_\nu(1)]\tau\Delta_H'/K$, to keep $[E_\nu(\infty) - E_\nu(1)]\tau$ a constant. Reproduction of the size dependence of the spectral peak positions yields the values as given in Table 1 based on the extreme situations of $\tau = 1$ and 3. Although no immediate information regarding the growth pattern was available in the current experiment, the presence of the B peak in Figure 4 for the 2 ML spectrum suggests that $\tau = 3$ is possible. Because of the limitation of growth pattern identification, we can only suggest an energy range of $E_\nu(1) = 851.10-852.49$ eV instead of an exact value. Metals deposited on oxide or carbon substrates form the discontinuous structures, but the exact shape cannot be affirmed from the APECS. However, we address the possibilities in terms of thin plate ($\tau = 1$) and island ($\tau = 3$). This uncertainty leads to the uncertainty of the $E_\nu(1)$ value, requiring further confirmation by scanning tunneling microscopy characterization. Fortunately, the uncertainty does not invalidate the model's method of approach. An extended Wagner plot of the M versus L levels' energy shift given in Figure 5c renders a gradient of unity, suggesting no chemical contamination of the specimen by the TiO_2 substrate.

One may be concerned about the interface contribution to the measurement because of the possible bond contraction and band nature alteration.[24] In the current situation, the interface effect can be assumed to be the same for all the Ni films and hence only offsets the calculated values. Furthermore, if oxidation of Ni were to occur, it would offset the main peak by 1.1 eV[29] and produce a satellite at energy slightly higher than the main peak—both are not observed in the measured spectra. This conclusion corresponds to that deduced purely from the experimental conditions; that is, oxidation of Ni can hardly happen at temperatures below 370 K.[15] Therefore, an interface contribution is negligible for metal on an oxide surface in the BOLS calculations. However, for metal films growing on a metallic substrate, an interface relaxation and alloying such as Cu deposited on a Pd surface[31] may contribute to the energy level shifts, and the relaxation and the metal interdiffusion may extend to more atomic layers[24] than just the outermost three. This effect will be studied in future work.

D. More Evidence for Skin-Depth Quantum Trapping. Our derived information suggests that the observed energy shifts result from the size-induced lattice strain and the associated skin-depth quantum trapping for small clusters or surface interlayer relaxation of a bulk solid, which agrees with the previously recommended mechanism of surface interlayer strain and charge densification.[32–34] The consequent resonant diffraction of the incident irradiation light due to the surface bond contraction would take full responsibility for the positive core-level shift. It has been identified that a 12% contraction of the first layer spacing leads to a 0.50 eV positive shift of the Nb(001)-$3d_{3/2}$ level,[32] while a (10 ± 3)% contraction of the first layer spacing caused the Ta(001)-$4f_{5/2(7/2)}$ level to shift positively by 0.75 eV.[34] For Cu_{18} and Ni_{18} atomic clusters, calculations[30] suggested that the binding energies undergo 0.7−0.8 eV positive shifts when the average strain of the clusters is increased from zero to 6%. A combination of scanning tunneling microscopy/spectroscopy measurements and density functional theory calculations has revealed that the mean lattice constant of Co nanoislands deposited on copper substrates contracts by 6% from the bulk value of 0.251 to 0.236 nm when one moves from the center to the edge of the nanoislands.[35] An apparent energy shift of ~0.2 eV of the occupied valence states has been detected when the island size is reduced from 22.5 to 4.8 nm. Most strikingly, Matsui et al.[36] has recently discovered that the Ni-2p levels of the outermost three atomic layers shift positively and discretely to a higher binding energy, with the outermost atomic layer shifting the most. Hence, from the electronic structure point of view, the surface consists of three atomic layers. Earlier experiments using dynamic low-energy diffraction revealed that the first layer spacing of the Ni(110) surface contracts by 9.8 ± 1.8% with respect to the bulk value.[37] These findings agree with the findings of the coordination dependence of Au−Au bond contraction[20] that extends only to the outermost two interatomic spacings of the Au nanocrystals. The extent of bond contraction is insensitive to the type of substrate support.[38] These findings are consistent with the currently reported results and corroborate the BOLS correlation mechanism.

V. Conclusion

The correlation between the Auger kinetic energy and the APECS involved L and M lines has been established, showing that the energy shift of the Auger parameter is twice that of the 3d level. A combination of the new degree of freedom of solid size, the APECS technique, and the BOLS correlation mechanism has allowed us to obtain deeper insight into the physical origin for the size-induced energy shifts of the Ni-2p and Ni-3d bands with derived information regarding the Auger kinetic energy, the 2p and 3d energies for an isolated Ni atom, and their energy shifts upon bulk formation. The consistency between theoretical calculations and measurements of the lattice strain and core level shifts suggests that the size-induced change is dominated by the broken-bond-induced local strain and quantum trapping in the surface of skin depth, while atoms in the core of the sample behave as they do in a bulk sample. The accuracy of the derived information is subject to the precision of solid size and shape determination. The developed approach not only provides the means of the intra-atomic trapping and interatomic binding energy estimation but also amplifies the capability of the existing APECS technique.

Acknowledgment. Financial support from Nanyang Technological University and the Agency for Science, Technology and Research, Singapore, and the Nature Science Foundation (No. 10772157) of China is acknowledged.

References and Notes

(1) Sun, C. Q. *Prog. Solid State Chem.* **2007**, *35*, 1.
(2) Chen, M. S.; Goodman, D. W. *Science* **2004**, *306*, 252.
(3) Sun, C. Q.; Li, C. M.; Li, S.; Tay, B. K. *Phys. Rev. B* **2004**, *69*, 245402.
(4) Reif, M.; Glaser, L.; Martins, M.; Wurth, W. *Phys. Rev. B* **2005**, *72*, 155405.
(5) Aruna, I.; Mehta, B. R.; Malhotra, L. K.; Shivaprasad, S. M. *J. Appl. Phys.* **2008**, *104*, 064308.
(6) Mann, A. K.; Varandani, D.; Mehta, B. R.; Malhotra, L. K.; Shivaprasad, S. M. *J. Nanosci. Nanotech.* **2005**, *5*, 1858.
(7) Balamurugan, B.; Maruyama, T. *Appl. Phys. Lett.* **2006**, *89*, 033112.
(8) Balamurugan, B.; Maruyama, T. *J. Appl. Phys.* **2007**, *102*, 034306.
(9) Suprun, S. P.; Fedosenko, E. V. *Semiconductors* **2007**, *41*, 590.
(10) Kim, S.; Kim, M. C.; Choi, S. H.; Kim, K. J.; Hwang, H. N.; Hwang, C. C. *Appl. Phys. Lett.* **2007**, *91*, 103113.
(11) Wertheim, G. K.; Dicenzo, S. B.; Buchanan, D. N. E. *Phys. Rev. B* **1986**, *33*, 5384.
(12) Aiyer, H. N.; Vijayakrishnan, V.; Subbanna, G. N.; Rao, C. N. R. *Surf. Sci.* **1994**, *313*, 392.
(13) (a) Vijayakrishnan, V. A.; Chainani, A.; Sarma, D. D.; Rao, C. N. R. *J. Phys. Chem.* **1992**, *96*, 8679. (b) Mason, M. G. In *Cluster Models for Surface and Bulk Phenomena*; Pacchioni, G., Ed.; Plenum: New York, 1992.
(14) Zafeiratos, S.; Kennou, S. *Surf. Sci.* **2001**, *482*, 266.
(15) Winkler, A.; Borchert, H.; Al-Shamery, K. *Surf. Sci.* **2006**, *600*, 3036.
(16) Moretti, G. J. *Electron Spectrosc. Relat. Phenom.* **1998**, *95*, 95.
(17) Wagner, C. D. *Anal. Chem.* **1972**, *44*, 967.
(18) Sun, C. Q. *Prog. Mater. Sci.* **2003**, *48*, 521.
(19) Sun, C. Q. *Phys. Rev. B* **2004**, *69*, 045105.
(20) Huang, W. J.; Sun, R.; Tao, J.; Menard, L. D.; Nuzzo, R. G.; Zuo, J. M. *Nat. Mater.* **2008**, *7*, 308.
(21) Omar, M. A. *Elementary Solid State Physics: Principles and Applications*; Addison-Wesley: New York, 1993.
(22) Marcus, P.; Hinnen, C. *Surf. Sci.* **1997**, *392*, 134.
(23) Yang, D. Q.; Sacher, E. *J. Phys. Chem. B* **2005**, *109*, 19329.
(24) Sun, C. Q. *Prog. Mater. Sci.* **2009**, *54*, 179.
(25) Liu, R. S. UHV deposition of Co thin films on low index Si surfaces. Ph.D. Thesis, 2003.
(26) Kara, A.; Rahman, T. S. *Phys. Rev. Lett.* **1998**, *81*, 1453.
(27) Woltersdorf, J.; Nepijko, A. S.; Pippel, E. *Surf. Sci.* **1981**, *106*, 64.
(28) Lamber, R.; Wetjen, S.; Jaeger, N. I. *Phys. Rev. B* **1995**, *51*, 10968.
(29) Nesbitt, H. W.; Legrand, D.; Bancroft, G. M. *Phys. Chem. Miner.* **2000**, *27*, 357.
(30) Richter, B.; Kuhlenbeck, H.; Freund, H. J.; Bagus, P. S. *Phys. Rev. Lett.* **2004**, *93*, 026805.
(31) Khanuja, M.; Mehta, B. R.; Shivaprasad, S. M. *Thin Solid Films* **2008**, *516*, 5435.
(32) Fang, B. S.; Lo, W. S.; Chien, T. S.; Leung, T. C.; Lue, C. Y.; Chan, C. T.; Ho, K. M. *Phys. Rev. B* **1994**, *50*, 11093.
(33) Balasubramanian, T.; Andersen, J. N.; Wallden, L. *Phys. Rev. B* **2001**, *64*, 205420.
(34) Bartynski, R. A.; Heskett, D.; Garrison, K.; Watson, G.; Zehner, D. M.; Mei, W. N.; Tong, S. Y.; Pan, X. *J. Vac. Sci. Technol., A* **1989**, *7*, 1931.
(35) Mironets, O.; Meyerheim, H. L.; Tusche, C.; Stepanyuk, V. S.; Soyka, E.; Zschack, P.; Hong, H.; Jeutter, N.; Felici, R.; Kirschner, J. *Phys. Rev. Lett.* **2008**, *100*, 096103.
(36) Matsui, F.; Matsushita, T.; Kato, Y.; Hashimoto, M.; Inaji, K.; Guo, F. Z.; Daimon, H. *Phys. Rev. Lett.* **2008**, *100*, 207201.
(37) Xu, M. L.; Tong, S. Y. *Phys. Rev. B* **1985**, *31*, 6332.
(38) Miller, J. T.; Kropf, A. J.; Zha, Y.; Regalbuto, J. R.; Delannoy, L.; Louis, C.; Bus, E.; van Bokhoven, J. A. *J. Catal.* **2006**, *240*, 222.

JP902405Q